Monitoring microvascular perfusion variations with laser speckle contrast imaging using a view-based temporal template method

Mohammad Zaheer Ansari, Eun-Jeung Kang, Mioara Manole, Jens Dreier, Anne Humeau-Heurtier

HHS Public Access

Author manuscript

Microvasc Res. Author manuscript; available in PMC 2019 January 30.

Published in final edited form as:

Microvasc Res. 2017 May ; 111: 49–59. doi:10.1016/j.mvr.2016.12.004.

Monitoring microvascular perfusion variations with laser speckle contrast imaging using a view-based temporal template method

Mohammad Zaheer Ansari[a,*], **Eun-Jeung Kang**[b,c,d], **Mioara D. Manole**[e], **Jens P. Dreier**[b,c,d], and **Anne Humeau-Heurtier**[f]

[a]Department of Physics, Cambridge Institute of Polytechnic, Baheya, Angara, Ranchi - 835103, Jharkhand, India

[b]Department of Experimental Neurology, Charité University Medicine Berlin, Charitéplatz 1, 10117 Berlin, Germany

[c]Department of Neurology, Charité University Medicine Berlin, Charitéplatz 1, 10117 Berlin, Germany

[d]Center for Stroke Research, Charité University Medicine Berlin, Charitéplatz 1, 10117 Berlin, Germany

[e]University of Pittsburgh, Safar Center for Resuscitation Research, USA

[f]Univ Angers, LARIS — Laboratoire Angevin de Recherche en Ingénierie des Systèmes, Angers, France

Abstract

Purpose—Laser speckle contrast imaging (LSCI) continues to gain an increased interest in clinical and research studies to monitor microvascular perfusion. Due to its high spatial and temporal resolutions, LSCI may lead to a large amount of data. The analysis of such data, as well as the determination of the regions where the perfusion varies, can become a lengthy and tedious task. We propose here to analyze if a view-based temporal template method, the motion history image (MHI) algorithm, may be of use in detecting the perfusion variations locations.

Methods—LSCI data recorded during three different kinds of perfusion variations are considered: (i) cerebral blood flow during spreading depolarization (SD) in a mouse; (ii) cerebral blood flow during SD in a rat; (iii) cerebral blood flow during cardiac arrest in a rat. Each of these recordings was processed with MHI.

Results—We show that, for the three pathophysiological situations, MHI identifies the area in which perfusion evolves with time. The results are more easily obtained compared with a visual

[*]Corresponding authors, mohamedzaheer1@gmail.com.

Disclosure of Conflicts of Interest

The authors have no relevant conflicts of interest to disclose.

inspection of all of the frames constituting the recordings. MHI also has the advantage of relying on a rather simple algorithm.

Conclusions—MHI can be tested in clinical and research studies to aid the user in perfusion analyses.

Keywords

cerebral blood flow; microcirculation; motion history image; biomedical signal processing

1. Introduction

In the clinical and research fields, the monitoring of microvascular perfusion is currently used for the diagnosis of microvascular pathologies, to analyze the effect of a drug, or to better understand a physiological phenomenon.[1,2] Indeed, microcirculatory dysfunction plays a key role in the pathophysiology of various diseases and may impact patient outcome. Several laser-based technologies have been proposed to monitor microvascular perfusion: laser Doppler flowmetry (LDF), laser Doppler imaging (LDI), and laser speckle contrast imaging (LSCI), to cite the three probably most well-known.[3–5] Compared with (single-point) LDF, LDI has the advantage of being contactless and gives bidimensional maps of the perfusion. Compared with LDI, LSCI has the advantage of being full-field and provides high temporal and spatial resolutions. Moreover, the measures are highly reproducible and the instrument can be made with low-cost devices.[6–9] LSCI has been used in a variety of applications.[1,10,11] However, one of the drawbacks of LSCI is that it leads to a large amount of data: one image is acquired at the sampling frequency rate (often several images/s); the recording can last several minutes to hours to assess the perfusion variations following a stimulus or a pathological process. Because of this, the analysis of a stack composed of many laser speckle contrast images becomes a lengthy and tedious task. For the user, the goal of this stack analysis can be, e.g., the detection of the regions where the perfusion varies. To aid in performing this task, two algorithms have recently been proposed: the generalized difference (GD) algorithm[12] and the motion history image (MHI) algorithm.[13] Thus far, to the best of our knowledge, the MHI algorithm has been applied to LSCI data (microvascular blood flow data) to solely monitor mouse cerebral blood flow during spreading depolarization (SD).[13]

Therefore, the goal of this investigation was to analyze if the MHI algorithm applied to a variety of LSCI data can effectively help in detecting the places where the perfusion variations occur. Three different kinds of recordings were processed with MHI. The results were analyzed and discussed. A conclusion on the use of MHI for assessment of microvascular perfusion is proposed.

2. Materials and Methods

2.1 Laser speckle contrast imaging

LSCI is a recently commercialized imaging modality that is based on photons-tissue interactions. It is used for relative and qualitative imaging of blood flow and perfusion. The principle of the technique is as follows: the tissue under study is illuminated by a laser

light[14–16] and the backscattered light is imaged onto a camera where it produces a random interference pattern known as speckle. Moving scattering particles in the tissue (e.g., red blood cells) cause fluctuations in the interference, which appear as intensity variations on the camera.[14–16] With these intensity variations of the speckle pattern, the exposure time of the camera (typically 1 to 10 ms) will lead to a blurred speckle pattern. The spatial blurring of the speckle pattern is then quantified by computing the contrast of the speckle images; the contrast is lower in regions with movement than in static regions. The perfusion map is determined from the contrast image (the perfusion is inversely proportional to the contrast). In our work, the images processed with MHI correspond to the perfusion images. These perfusion images were generated directly inside the imager from the raw contrast data. The perfusion images were then exported with the software associated with the device and converted to a format readable with MATLAB Release 2008a (The MathWorks, Inc., Natick, Massachusetts, United States) for post-acquisition processing.

2.2 Image processing method

Previous publications suggested approaches that recognize motion in an image sequence.[17–19] Among these methods, MHI has been proposed as a view-based temporal template method.[20] The procedure gives rise to a new image (so-called MHI) where the pixel intensity is a function of the temporal history of motion at the corresponding pixel in the image sequence: the MHI is a scalar-valued image where intensity is a function of recency of motion (blue to red; red for the most recent motion). The more recently moving pixels are brighter. A MHI H_τ is computed as:[20]

$$H_\tau(x,y,t) = \begin{cases} \tau & \text{if} \quad \psi(x,y,t) = 1 \\ \max\left(0, H_\tau(x,y,t-1) - 1\right) & \text{otherwise,} \end{cases} \quad (1)$$

where (x,y) and t are the position and time, respectively, τ is the duration (temporal extent of the movement, in terms of frames), and $\Psi(x,y,t)$ is a binary image sequence indicating regions of motion. This function (also named update function[21]) is called for every new video frame analyzed in the sequence. For many applications, Ψ can be generated with image-differencing:[20]

$$\Psi(x,y,t) = \begin{cases} 1 & \text{if} \quad |I(x,y,t) - I(x,y,t-1)| \geq \xi \\ 0 & \text{otherwise} \end{cases}, \quad (2)$$

where $I(x,y,t)$ is the intensity value of pixel location with coordinate (x,y) at the tth frame of the image sequence, and ξ is a threshold. ξ needs to be chosen in such a way that it tends to see motion in the right places and not too much noise.

One of the advantages of MHI is that a range of times can be encoded in a single frame. The concept of MHI has been used in a variety of applications.[21] In our work, MHI was implemented with the MATLAB Release 2008a (The MathWorks, Inc., Natick, Massachusetts, United States) software.

2.3 Data acquisition

2.3.1 Cerebral blood flow monitoring during spreading depolarization in a mouse—We first analyzed in greater depth[13] cerebral blood flow of a mouse during SD. The experiment was done in compliance with institutional guidelines and international standards on animal welfare and was approved according to local and national regulations for animal care and use for research purposes. During the preparation and the acquisition, the body temperature was continuously measured and maintained at 37.8°C by the use of an automatic controlled homeothermic blanket system. The mouse was anesthetized with isoflurane (2.5% induction, 1.5–2% during surgery) in 70% N_2O and 30% O_2. It was placed in a stereotaxic frame and the skin was removed above both hemispheres. After the end of the preparation, isoflurane anesthesia was reduced to 1.1–1.2%.[13] The cerebral blood perfusion was recorded on the two hemispheres of the mouse, through the skull.[12,13] For the perfusion measurement, a PeriCam PSI System (Perimed, Sweden) with a laser wavelength of 785 nm and an exposure time of 6 ms was used. The sampling frequency was 0.1 Hz. The distance between the camera and the skull was set to 10.4 cm. The perfusion images had a resolution of 0.02 mm. The perfusion variations were monitored during a pinprick in the right hemisphere that induced SD.

2.3.2 Cerebral blood flow monitoring during SD in a rat—The aim of the second acquisition was to monitor the cerebral blood flow of a rat, during SD. The animal experiments were approved by Governmental Animal Care and use Committee (Landesamt für Arbeitsschutz, Gesundheitsschutz und technische Sicherheit Berlin). A 12-week old Wistar Kyoto rat (WKY), bred in our own animal facility (Forschungseinrichtungen für Experimentelle Medizin (FEM) Charité), was anesthetized with 100 mg/kg thiopental-sodium intraperitoneally (Trapanal, BYK Pharmaceuticals, Konstanz, Germany), tracheomized and artificially ventilated (Effenberger Rodent Respirator, Effenberger med.-Techn. Gerätebau, Pfaffing, Germany). Vital parameters including end-expiratory CO_2 pressure (Heyer Artema MM 204, Artema Medical AB, Sweden) and body temperature (Homeothermic Blanket Control Unit, ME, USA) were monitored during the entire experiment. A cannulation of the left femoral artery was performed for monitoring the systemic arterial blood pressure (Pressure Monitor BP-1, World Precision Instruments, Berlin, Germany). Blood gases including arterial partial pressure of O_2 (PaO_2), arterial partial pressure of CO_2 ($PaCO_2$) and pH (ABL 80 flex, Radiometer, Willich, Germany) were analyzed before and after the recording. Thiopental was additionally administered when the animal responded to tail pinch with movement and blood pressure changes, indicating waking state. The rat was euthanized shortly after the experiment by intravenous application of concentrated KCl solution.

As described previously,[22–23] a cranial window was implanted over the somatosensory cortex and closed by a cover slip. The dura mater was removed in the window area. To measure changes of subdural direct current (DC) potential and regional cerebral blood flow (rCBF) during SD, an Ag/AgCl electrode was placed between the cover slip and the cortex and a laser speckle contrast imager (PeriCam PSI, Perimed AB, Järfälla, Sweden) was located over the window. The data were recorded with a sampling frequency of 0.5 Hz. The distance between the camera and the skull was set to 10.1 cm. The perfusion images had a

resolution of 0.02 mm. Artificial cerebrospinal fluid (aCSF) was topically applied to the brain cortical surface containing in mM: 127.5 NaCl, 24.5 $NaHCO_3$, 6.7 urea, 3.7 glucose, 3 KCl, 1.5 $CaCl_2$, and 1.2 $MgCl_2$. The aCSF was aerated with a gas mixture containing 6% O_2, 5.9% CO_2, and 87.5% N_2 to ensure physiological levels of pO_2 (90–130 mmHg), pCO_2 (35–45 mmHg) and pH (7.35–7.45). A small frontal burr hole was implanted to elicit SD using a bipolar electrode with two insulated stainless steel wires.

The Ag/AgCl electrode was connected to a differential amplifier (Jens Meyer, Munich, Germany) and signals were converted from analog to digital using a Power 1401 (Cambridge Electronic Design Limited, Cambridge, UK). Electrical stimulation was generated by Master-8 (A.M.P.I. Instruments, Jerusalem, Israel) connected to an isolator (Stimulus Isolation Unit SIU-102, Warner Instruments, CT, USA). The stimulation was performed in the right hemisphere. It followed an empirical protocol with an exponential function until an SD occurred.

2.3.3 Cerebral blood flow monitoring during cardiac arrest in rat—For the third acquisition, we studied cerebral blood flow in a postnatal day 17 rat at baseline, during asphyxia, cardiac arrest, and post-resuscitation. The experiment was done in compliance with institutional guidelines and international standards on animal welfare and approved according to local and national regulations for animal care and use for research purposes (University of Pittsburgh, USA). We used an established cardiac arrest model and assessment of cerebral perfusion as described previously.[24] Briefly, a postnatal day 17 rat was initially anesthetized with isoflurane in a Plexiglas until unconscious. The trachea was then intubated with an 18-gauge angiocatheter, and femoral arterial and venous catheters were placed. Intravenous anesthesia was initiated using fentanyl and vecuronium intravenous infusions at 50 μg/kg and 5 mg/kg, respectively, and isoflurane was discontinued. The rat was placed prone in a stereotaxic frame and a midline scalp incision was performed to expose the skull. Cerebral perfusion was measured through the intact skull and was recorded continuously at baseline, during, and after cardiac arrest. Acquisition of the perfusion data was accomplished with a PeriCam PSI System (Perimed, Sweden) with a laser wavelength of 785 nm, exposure time of 6 ms, and sampling frequency of 10 Hz. The distance between the camera and the skull was set to 17.3 cm. The perfusion images had a resolution of 0.16 mm. Asphyxial cardiac arrest was induced by disconnecting the tracheal tube from the ventilator for 9 minutes. Resuscitation was performed by re-initiating mechanical ventilation with 100% oxygen, chest compression, and infusion of epinephrine and bicarbonate (0.005 mg/kg and 1mEq/kg, respectively). The temperature was maintained at 37°C, and the heart rate, and mean arterial pressure were monitored throughout the experiment. Arterial blood gases were obtained at baseline and at 10 and 30 min after cardiac arrest. The pCO_2 was maintained between 35 and 45 mmHg by adjusting the ventilation rate and tidal volumes.

3. Results

3.1 Monitoring the spreading depolarization in the two hemispheres of a mouse

An example of perfusion map of the two hemispheres (before the pinprick) for the mouse is shown in Fig. 1. The time evolution of the perfusion in two regions of interest (ROIs) is also

represented. From this figure (right panel), we observe that the perfusion in the hemisphere where no pinprick was performed is rather constant (see blue curve). However, in the hemisphere where the pinprick was performed, a SD is observed. This is characterized by changes in regional cerebral blood flow. This is also shown in Fig. 2 where LSCI images at different time points are represented. Fig. 3 shows the corresponding MHIs. Each MHI was computed from LSCI perfusion images around the frames shown in Fig. 2. Fig. 3 reveals the locations where perfusion changes occur. This is much more visible than in the raw LSCI data shown. We observed that the perfusion variations first occur at the pinprick location and then propagate in the gray matter of the central nervous system.

3.2 Monitoring the spreading depolarization followed by perfusion variations in a rat

Figure 4 represents the perfusion map of the somatosensory cortex for the rat, before and after the stimulation inducing SD. We note that the perfusion changes are somewhat less obvious than in the mouse. The perfusion variations are shown in Fig. 5 for two ROIs. Fig. 6 shows the corresponding MHIs. From the latter, we observe that there are perfusion variations but no propagation is noted, as it was the case for the mouse (see Fig. 3).

3.3 Assessment of cerebral blood flow changes after cardiac arrest in a rat

Different perfusion maps recorded before, during, and after the cardiac arrest for the 17 day old rat are shown in Fig. 7. The time evolution of the perfusion for two ROIs is shown in Fig. 8. At the onset of asphyxia, cerebral perfusion decreases progressively, culminating with the absence of perfusion during cardiac arrest. Perfusion is restored during and after resuscitation. However perfusion is decreased compared with baseline after resuscitation from cardiac arrest (see Figs. 7 and 8). Fig. 9 shows the corresponding MHIs. From the latter, we observe the perfusion variations evolution (much more clearly than in Fig. 7).

4. Discussion

We demonstrated the feasibility of detecting perfusions variations by applying MHI analysis to data acquired using LSCI. Using MHI, we examined the major fluctuations of cerebral blood flow before, during, and after several stimulations in mice and rats.

We initially assessed SD in rodents. SD has been described as a propagating wave with a velocity of approx. 3 mm/min in the gray matter of the central nervous system, and is characterized by sustained depolarization of neurons and depression of brain electrical activity.[25] The underlying mechanism of SD is a massive disturbance of ion homeostasis between the intracellular and extracellular compartments. This mismatch of ion flux across the cell membrane is attributed to insufficient ATP-dependent sodium and calcium pump activity, which cannot compensate for the massive cation influx into cells. To restore the ion homeostasis, it is necessary to recruit additional sodium and calcium pumps, an energy-dependent process. During SD, CBF increases in healthy brain by more than 100% to compensate for the increased energy demand.[25] This so-called spreading hyperemia is sometimes preceded by a shallow initial hypoperfusion, and it is followed by a moderate hypoperfusion (spreading oligemia), lasting for up to two hours.[26] In spite of mild regional cerebral blood flow reduction and increase in the cerebral metabolic rate of oxygen during

spreading oligemia,[27] SD does not lead to histological damage in healthy brain tissue.[28] This pattern of regional cerebral blood flow changes associated with SD is observed in the naïve cortex of almost all investigated mammals, including rats, cats, and humans.[26] SD is different in mice compared to other mammals, such as rats. In the mouse, the cerebrovascular response to SD begins with pronounced initial hypoperfusion, and is followed by a short peak that barely reaches baseline, followed by very prolonged cerebral blood flow reduction by about 60%.[29]

We also assessed the perfusion variations during cardiac arrest, which produces a global cerebral insult. During asphyxial cardiac arrest, a series of physiological changes occur, which culminate with cardiac arrest. Initially, hypoxia, hypotension, and hypercarbia cause progressive decrease in cerebral perfusion. Over a period of 1–3 minutes after the onset of asphyxia, cardiac contractility markedly decreases and cardiac arrest occurs. Cortical cerebral perfusion progressively decreases during the initial period of hypoxia and hypotension, and absence of cerebral perfusion is observed during cardiac arrest. During resuscitation, some cerebral perfusion is detected, whereas upon return of spontaneous circulation the perfusion increases and is gradually restored, yet remains below baseline levels for several hours. Cortical hypoperfusion postcardiac arrest is insult-duration dependent, and is more pronounced after longer durations of cardiac arrest.[30] Variability of cerebral reperfusion may also exist and could be detected using LSCI, evidencing the no-reflow phenomenon that occurs at the level of the capillary bed post-cardiac arrest. Decreased cortical perfusion after cardiac arrest is a multifactorial phenomenon, secondary to physiological and structural changes at the level of endothelial cells and perivascular glia.[31] In the current study we used an established and clinically relevant pediatric asphyxial cardiac arrest in immature, postnatal 17 day old rats. The 17 day old rats' skulls are thin, and LSCI imaging can be performed through the intact skull. In this model LSCI has the advantage of assessing perfusion noninvasively and continuously over a large cortical area at baseline, during cardiac arrest, and post-resuscitation, and thus is important for the development of vascular-targeted therapeutic strategies for brain resuscitation after cardiac arrest.[24,32]

There are several advantages of the MHI technique. MHI technique for LSCI perfusion allows obtaining information on the temporal evolution of the perfusion variations. In clinical and research applications an ROI is often performed on the perfusion maps obtained by LSCI. In the respective ROI the perfusion is averaged and recorded serially over time. This breaks the bidimensional nature of the maps, and thus undermines the advantage of LSCI over other technique as monopoint LDF. When using MHI, no mean value is computed and a bidimensional image reflecting the perfusion variations with time is generated. The MHI technique can also be applied to study other perfusion variations on human skin and on larger areas (as performed previously for GD).[12] MHI could also be used to study perfusion variations during post-occlusive reactive hyperemia or induced by local heating. However, MHI is sensitive to any perfusion fluctuation. Therefore, to avoid perfusion variations due to movements of the subject, an adhesive opaque is required.[33,34]

In our work, different parameters have been used for data acquisition (different distances between the camera and the tissue, different image resolutions, and different sampling

frequencies). We must note that the distance between the camera and the tissue, and thus the perfusion image resolution, has an influence on MHI: MHI has the same resolution as the original LSCI data. The sampling frequency also has an influence on MHI: the higher the sampling frequency, the larger the number of frames necessary to target a given time interval. Thus, the quality of the resulting MHI can be enhanced by the proper adjustment of parameter values, particularly the level of threshold and the buffer size.[35] In a recent publication,[13] we have shown that the adjustment of the threshold value in MHI allows to reinforce the separation of distinct areas of activity (here perfusion areas). This is also illustrated with Fig. 10 where MHI generated with different threshold values and a buffer size of 6 are shown. Moreover, the buffer size in MHI determines the ability to get information linked with lower activities (here low perfusion variations), acting as a digital integrator.[35] Figure 11 shows MHI generated with different buffer sizes using a threshold value of 60. A buffer size of 12 highlights the lower activity as indicated by the arrow.

Compared with other algorithms such as GD, MHI has the advantage of providing information on the temporal evolution of perfusion variations, which GD cannot provide. In the case of MHI, the sampling frequency of the data is known and thus it could be possible to obtain a relation between the pixel values (colorbar) and the time points. Moreover, in our work the MHIs shown were obtained from substacks of images. This was performed to obtain a better visualization of the perfusion variations. Even with the choice of particular time points, MHI has the great advantage of leading to bidimensional maps of perfusion variations, which is not possible if an averaging is performed in ROIs and followed with time. However, it is worth noting that - if many time points are chosen - the MHI procedure becomes time consuming. An additional limitation is that MHI provides information on the pixels with variation in perfusion, but is not able to distinguish between perfusion increases and decreases. This is inherent to the algorithm and is a drawback for studies where perfusion can either increase or decrease in response to a stimulus at a particular time. Further work is necessary to overcome this limitation.

5. Conclusions

LSCI, a laser-based technology, is currently used to monitor microvascular perfusion. This technique generates large amount of data that requires analysis. To help the clinician or researcher in this task, our goal was to analyze if the MHI algorithm applied to a variety of LSCI data can help in detecting the locations with perfusion variations. Through the analysis of LSCI data recorded during different conditions, we showed that MHI can effectively identify areas with perfusion variations. Future work should focus on the choice of the optimal parameters used in the algorithm.

Acknowledgments

We thank Andreea V. Toader for her valuable assistance with editing the manuscript.

This manuscript was supported by the NIH grant R01HD075760 (MDM).

References

1. Allen J J, Howell K. Microvascular imaging: techniques and opportunities for clinical physiological measurements. Physiol Meas. 2014; 35:R91–R141. [PubMed: 24910968]
2. Kara A, Akin S, Ince C. Monitoring microcirculation in critical illness. Curr Opin Crit Care. 2016; 22:444–452. [PubMed: 27583585]
3. Humeau-Heurtier A, Guerreschi E, Abraham P, Mahé G. Relevance of laser Doppler and laser speckle techniques for assessing vascular function: state of the art and future trends. IEEE Trans Biomed Eng. 2013; 60:659–666. [PubMed: 23372072]
4. Bi R, Dong J, Poh CL, Lee K. Optical methods for blood perfusion measurement--theoretical comparison among four different modalities. J. Opt. Soc. Am. A Opt. Image Sci. Vis. 2015; 32:860–866. [PubMed: 26366910]
5. Cracowski JL, Roustit M. Current Methods to assess human cutaneous blood flow: an updated focus on laser-based-techniques. Microcirculation. 2016; 23:337–344. [PubMed: 26607042]
6. Puissant C, Abraham P, Durand S, Humeau-Heurtier A, Faure S, Lefthériotis G, Rousseau P, Mahé G. Reproducibility of non-invasive assessment of skin endothelial function using laser Doppler flowmetry and laser speckle contrast imaging. PLoS One. 2013; 8:e61320. [PubMed: 23620742]
7. Roustit M, Millet C, Blaise S, Dufournet B, Cracowski JL. Excellent reproducibility of laser speckle contrast imaging to assess skin microvascular reactivity. Microvasc Res. 2010; 80:505–511. [PubMed: 20542492]
8. Humeau-Heurtier A, Abraham P, Durand S, Mahé G. Excellent inter- and intra-observer reproducibility of microvascular tests using laser speckle contrast imaging. Clin Hemorheol Microcirc. 2014; 58:439–446. [PubMed: 24254582]
9. Richard LM, Kazmi SM, Davis JL, Olin KE, Dunn AK. Low-cost laser speckle contrast imaging of blood flow using a webcam. Biomed. Opt. Express. 2013; 4:2269–2283. [PubMed: 24156082]
10. Kazmi SM, Richards LM, Schrandt CJ, Davis MA, Dunn AK. Expanding applications, accuracy, and interpretation of laser speckle contrast imaging of cerebral blood flow. J. Cereb. Blood Flow Metab. 2015; 35:1076–1084. [PubMed: 25944593]
11. Paul DW, Ghassemi P, Ramella-Roman JC, Prindeze NJ, Moffatt LT, Alkhalil A, Shupp JW. Noninvasive imaging technologies for cutaneous wound assessment: A review. Wound Repair Regen. 2015; 23:149–162. [PubMed: 25832563]
12. Humeau-Heurtier A, Mahé G, Abraham P. Microvascular blood flow monitoring with laser speckle contrast imaging using the generalized differences algorithm. Microvasc. Res. 2015; 98:54–61. [PubMed: 25576743]
13. Ansari MZ, Humeau-Heurtier A, Offenhauser N, Dreier JP, Nirala AK. Visualization of perfusion changes with laser speckle contrast imaging using the method of motion history image. Microvasc. Res. 2016; 107:106–109. [PubMed: 27321386]
14. Briers JD, Webster S. Laser speckle contrast analysis (LASCA): a nonscanning, full-field technique for monitoring capillary blood flow. J Biomed Opt. 1996; 1:174–179. [PubMed: 23014683]
15. Boas DA, Dunn AK. Laser speckle contrast imaging in biomedical optics. J. Biomed. Opt. 2010; 15
16. Briers D, Duncan DD, Hirst E, Kirkpatrick SJ, Larsson M, Steenbergen W, Stromberg T, Thompson OB. Laser speckle contrast imaging: theoretical and practical limitations. J. Biomed. Opt. 2013; 18
17. Lun R, Zhao W. A survey of applications and human motion recognition with Microsoft kinect. Int. J. Pattern Recognit. Art. Intell. 2015; 29
18. Hapsari GC, Prabuwono AS. Human Motion Recognition in Real-time Surveillance System: A Review. Journal of Applied Sciences. 2010; 10(22):2793–2798.
19. Cédras C, Shah M. Motion-based recognition a survey. Image Vision Comput. 1995; 13:129–155.
20. Bobick AF, Davis JW. The recognition of human movement using temporal templates. IEEE Trans. Pattern Anal. Machine Intell. 2001; 23:257–267.

21. Ahad MAR, Tan JK, Kim H, Ishikawa S. Motion history image: its variants and applications. Machine Vision Appl. 2012; 23:255–281.
22. Dreier JP, Kleeberg J, Petzold G, Priller J, Windmuller O, Orzechowski HD, Lindauer U, Heinemann U, Einhaupl KM, Dirnagl U. Endothelin-1 potently induces Leao's cortical spreading depression in vivo in the rat: a model for an endothelial trigger of migrainous aura? Brain. 2002; 125:102–112. [PubMed: 11834596]
23. Oliveira-Ferreira AI, Milakara D, Alam M, Jorks D, Major S, Hartings JA, Lückl J, Martus P, Graf R, Dohmen C, Bohner G, Woitzik J, Dreier JP. Experimental and preliminary clinical evidence of an ischemic zone with prolonged negative DC shifts surrounded by a normally perfused tissue belt with persistent electrocorticographic depression. J. Cereb. Blood Flow Metab. 2010; 30:1504–1519. [PubMed: 20332797]
24. Shaik JS, Poloyac SM, Kochanek PM, Alexander H, Tudorascu DL, Clark RS, Manole MD. 20-Hydroxyeicosatetraenoic acid inhibition by HET0016 offers neuroprotection, decreases edema, and increases cortical cerebral blood flow in a pediatric asphyxial cardiac arrest model in rats. J. Cereb. Blood Flow Metab. 2015; 35:1757–1763. [PubMed: 26058691]
25. Dreier JP. The role of spreading depression, spreading depolarization and spreading ischemia in neurological disease. Nat. Med. 2011; 17:439–447. [PubMed: 21475241]
26. Dreier JP, Reiffurth C. The stroke-migraine depolarization continuum. Neuron. 2015; 86:902–922. [PubMed: 25996134]
27. Piilgaard H, Lauritzen M. Persistent increase in oxygen consumption and impaired neurovascular coupling after spreading depression in rat neocortex. J. Cereb. Blood Flow Metab. 2009; 29:1517–1527. [PubMed: 19513087]
28. Nedergaard M, Hansen AJ. Spreading depression is not associated with neuronal injury in the normal brain. Brain Res. 1988; 449:395–398. [PubMed: 3395856]
29. Ayata C, Shin HK, Salomone S, Ozdemir-Gursoy Y, Boas DA, Dunn AK, Moskowitz MA. Pronounced hypoperfusion during spreading depression in mouse cortex. J. Cereb. Blood Flow Metab. 2004; 24:1172–1182. [PubMed: 15529018]
30. Manole MD, Foley LM, Hitchens TK, Kochanek PM, Hickey RW, Bayir H, Alexander H, Ho C, Clark RS. Magnetic resonance imaging assessment of regional cerebral blood flow after asphyxial cardiac arrest in immature rats. J. Cereb. Blood Flow Metab. 2009; 29:197–205. [PubMed: 18827831]
31. Ames A 3rd, Wright RL, Kowada M, Thurston JM, Majno G. Cerebral ischemia. II. The no-reflow phenomenon. Am. J. Pathol. 1968; 52:437–453. [PubMed: 5635861]
32. Manole MD, Kochanek PM, Foley LM, Hitchens TK, Bayir H, Alexander H, Garman R, Ma L, Hsia CJ, Ho C, Clark RS. Polynitroxyl albumin and albumin therapy after pediatric asphyxial cardiac arrest: Effects on cerebral blood flow and neurologic outcome. J Cereb Blood Flow Metab. 2012; 32:560–569. [PubMed: 22126915]
33. Mahé G, Rousseau P, Durand S, Bricq S, Leftheriotis G, Abraham P. Laser speckle contrast imaging accurately measures blood flow over moving skin surfaces. Microvasc. Res. 2011; 81:183–188. [PubMed: 21156183]
34. Omarjee L, Signolet I, Humeau-Heutier A, Martin L, Henrion D, Abraham P. Optimisation of movement detection and artifact removal during laser speckle contrast imaging. Microvasc. Res. 2015; 97:75–80. [PubMed: 25261716]
35. Godinho RP, Silva MM, Nozela JR, Braga RA. Online biospeckle assessment without loss of definition and resolution by motion history image. Optics Lasers Eng. 2012; 50:366–372.

Highlights

- The motion history image (MHI) algorithm can be of help in detecting the perfusion variations locations.
- MHI stresses the area where perfusion evolves with time.
- MHI has the advantage of relying on a rather simple algorithm.
- MHI could now be used in clinical and research studies to help the user in perfusion analyses.

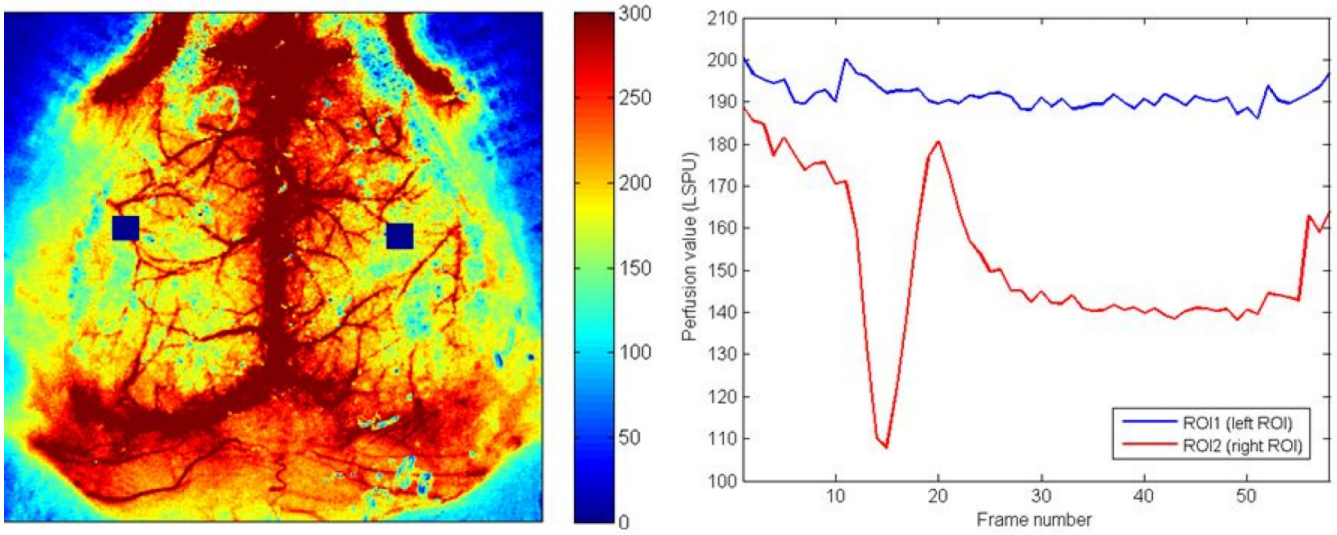

Fig. 1.

Left panel: LSCI perfusion map representing the two hemispheres of a mouse recorded through the skull (before the pinprick). The two blue squares represent two ROIs. Right panel: time evolution of the perfusion in the two ROI shown in the left panel. The pinprick has been performed in the right ROI.

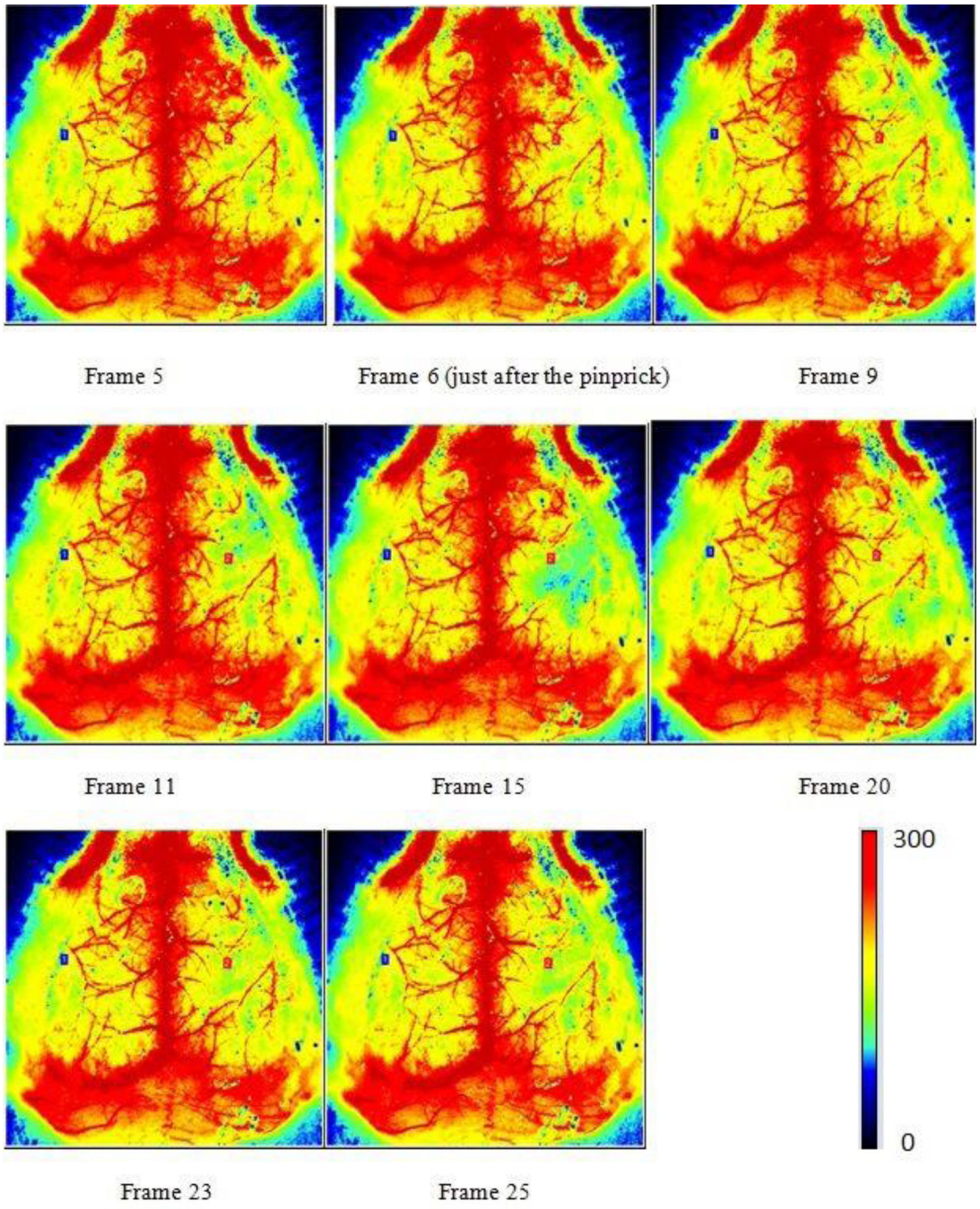

Fig. 2.
LSCI data before and after a pinprick inducing SD in the right hemisphere of a mouse. The frequency acquisition was 0.1 Hz.

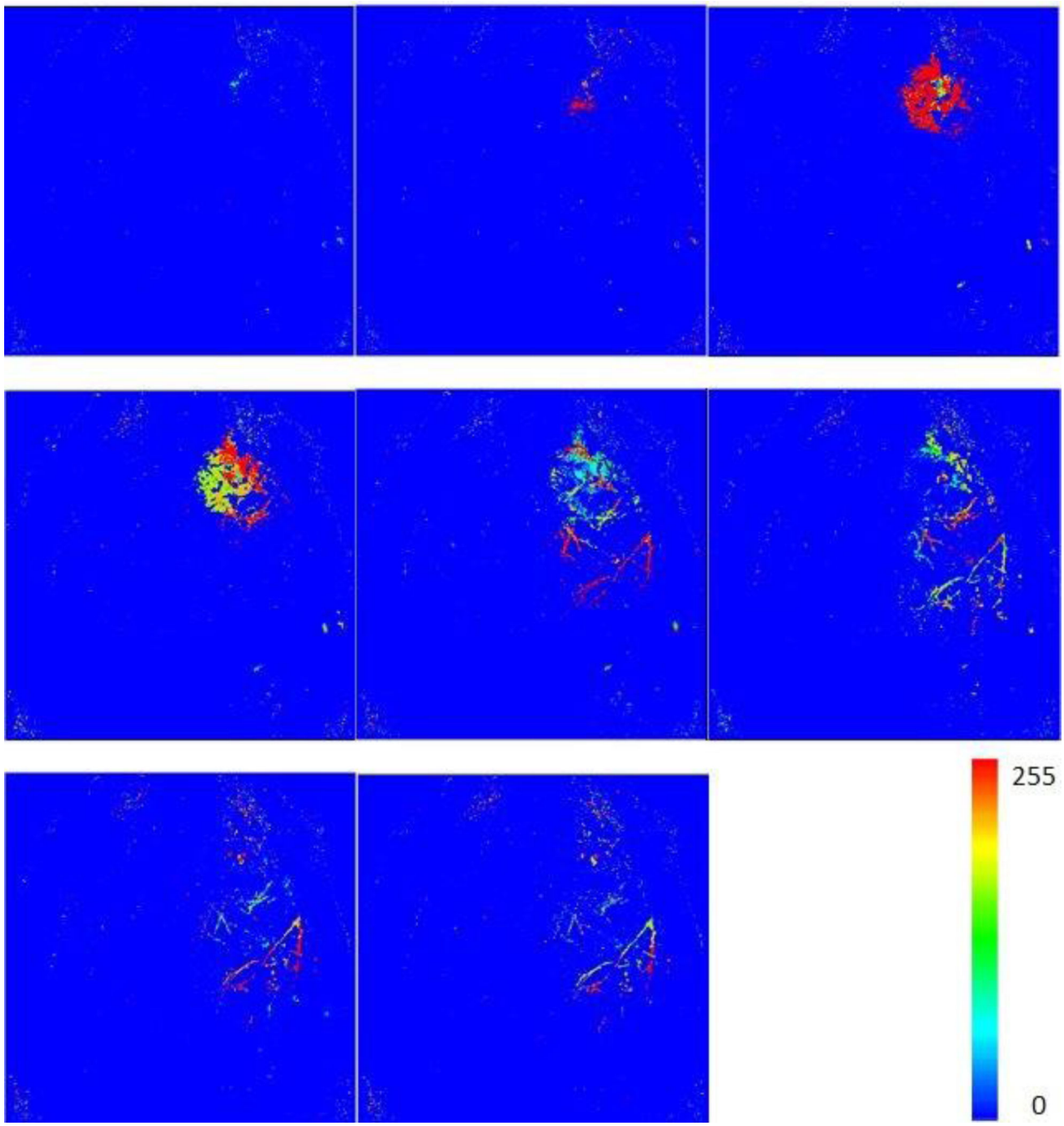

Fig. 3.

MHIs showing the fluctuations in regional cerebral blood flow of a mouse. The perfusion variations are induced by a pinprick generating SD. Each MHI was computed from a stack of LSCI perfusion images around particular time points shown in Fig. 2. For the computation of each MHI, we used a buffer of 6 (LSCI) images with a threshold value of 100.

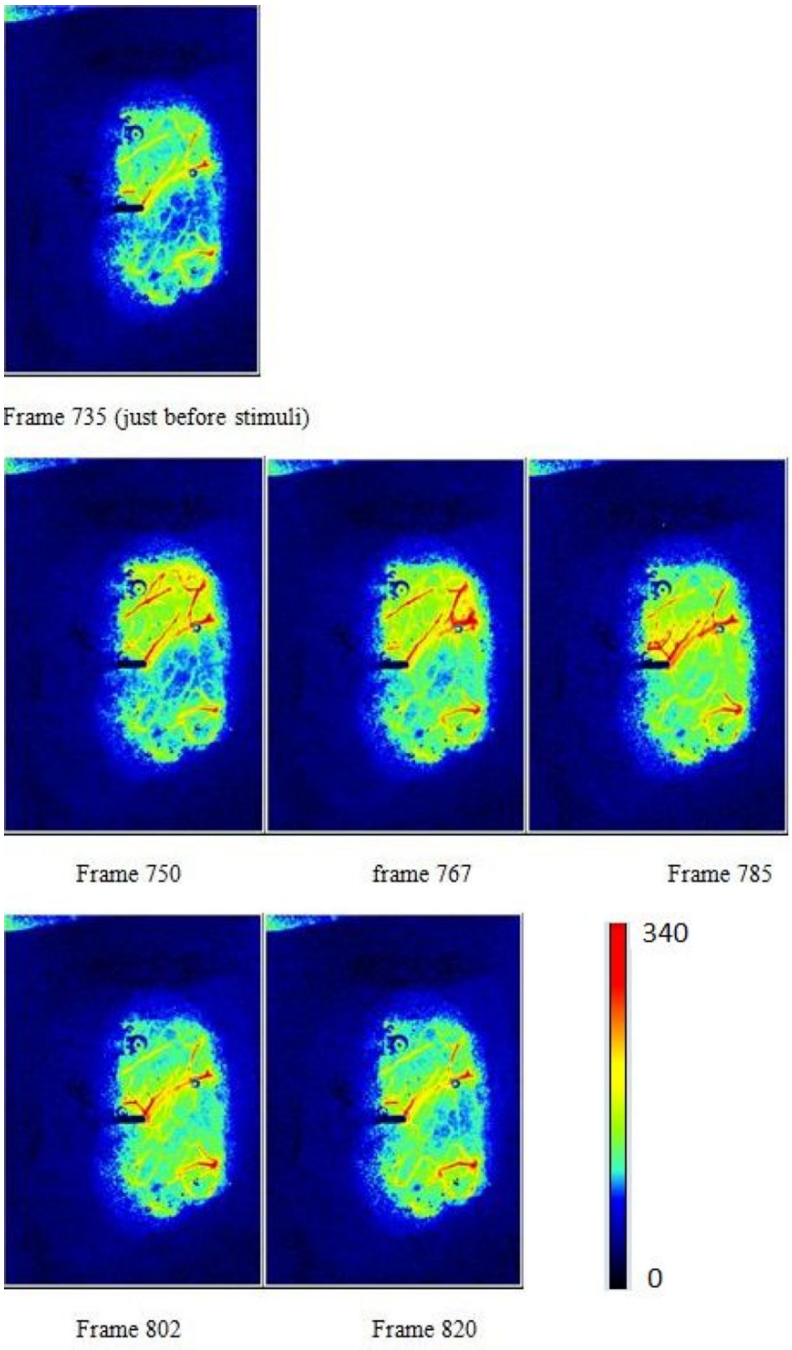

Fig. 4.

LSCI perfusion map of the somatosensory cortex for a rat, before and after a simulation inducing SD. The stimulation was performed around frame 740. The frequency acquisition was 0.5 Hz.

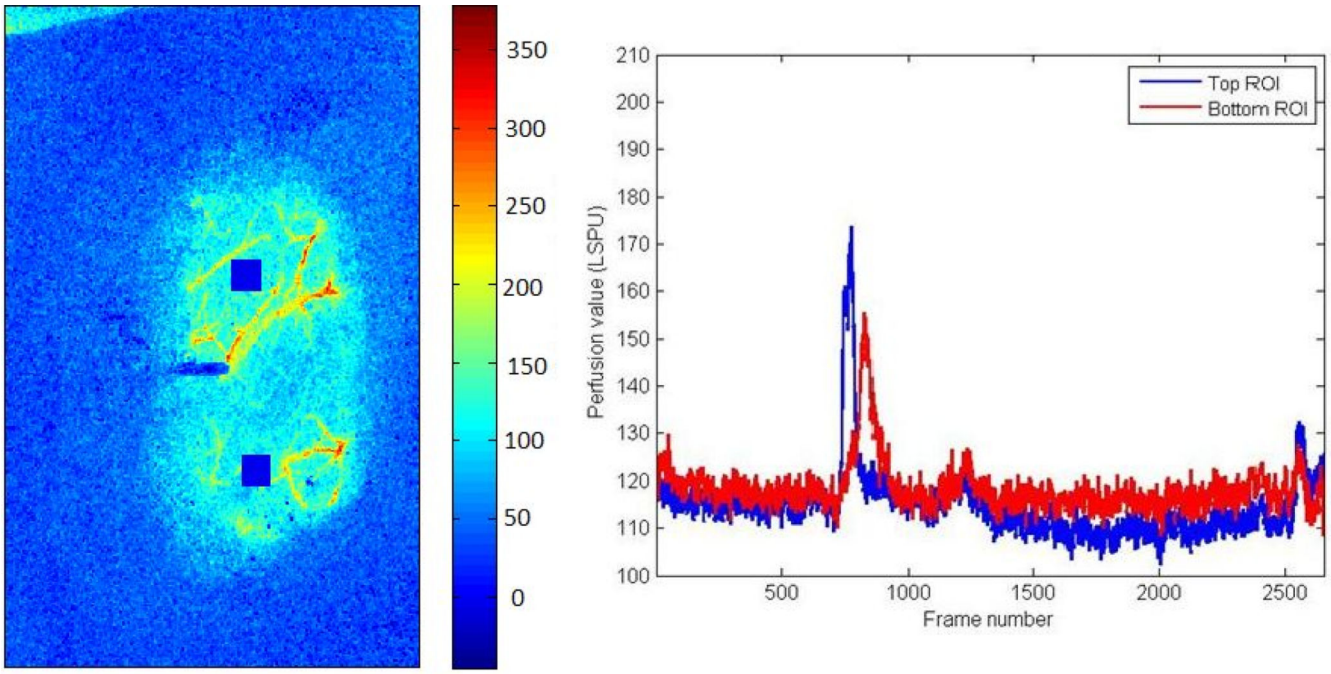

Fig. 5.

Left panel: two ROIs (blue squares) on a perfusion map representing the cerebral blood flow of a rat. Right panel: ROI perfusion evolution with time before, during, and after SD.

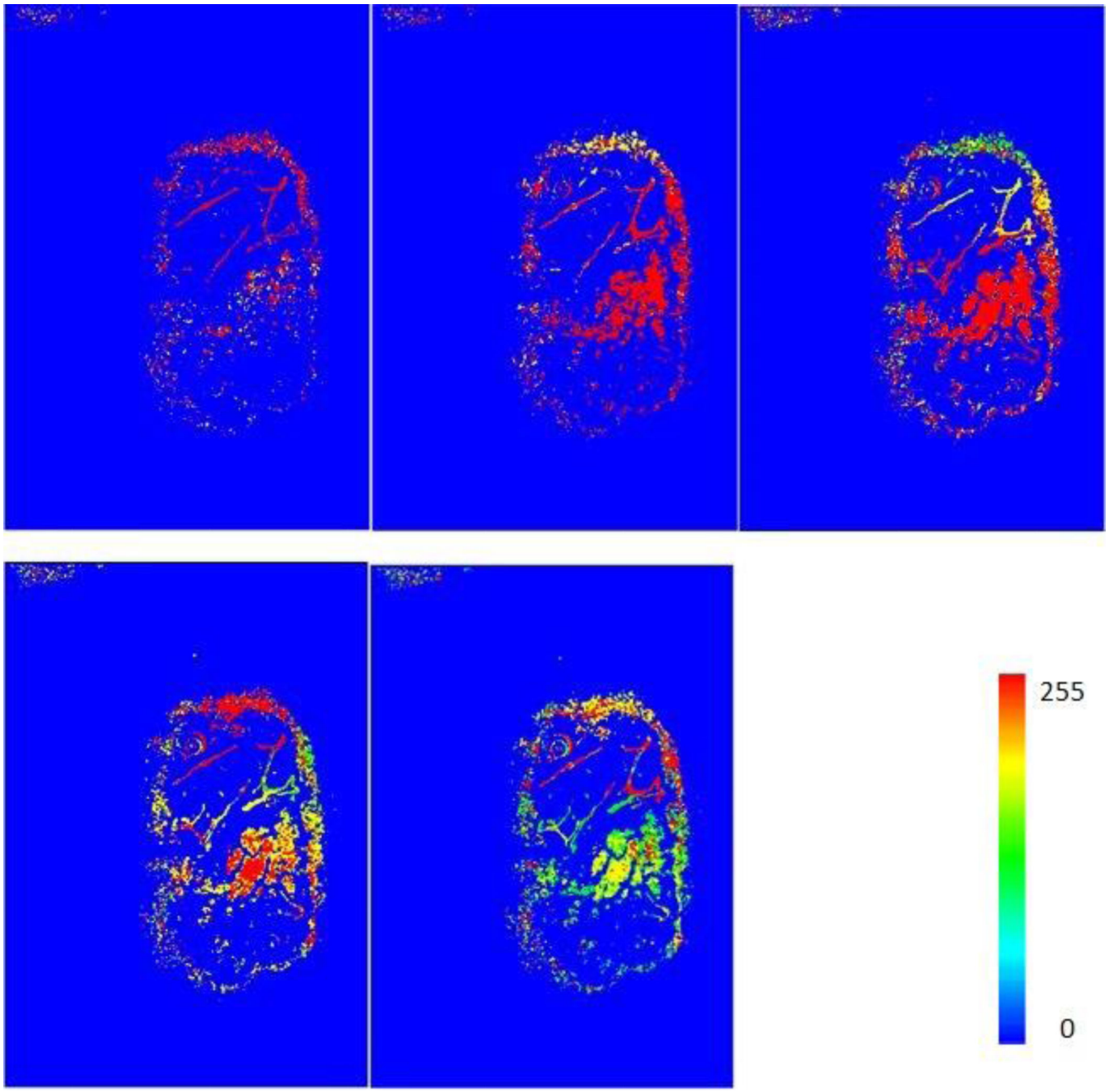

Fig. 6.

MHIs showing the fluctuations in regional cerebral blood flow of a rat. The perfusion variations are induced by a stimulation generating SD. Each MHI was computed from a stack of LSCI perfusion images around a particular time point shown in the two last lines of Fig. 4. For the computation of each MHI, the buffer size was 4, and the threshold value was 60.

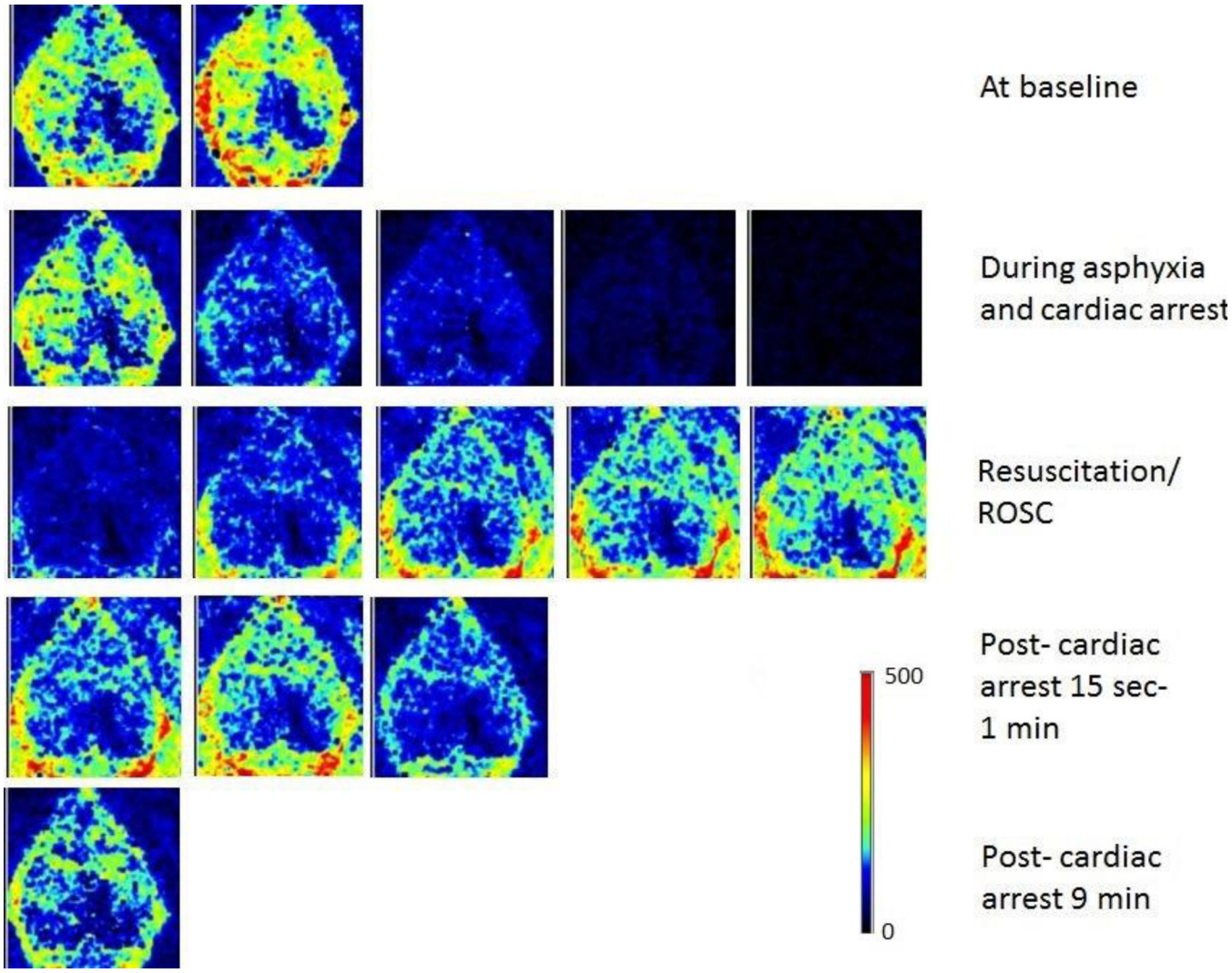

Fig. 7.
LSCI perfusion map of the rat cortex before, during, and after cardiac arrest.

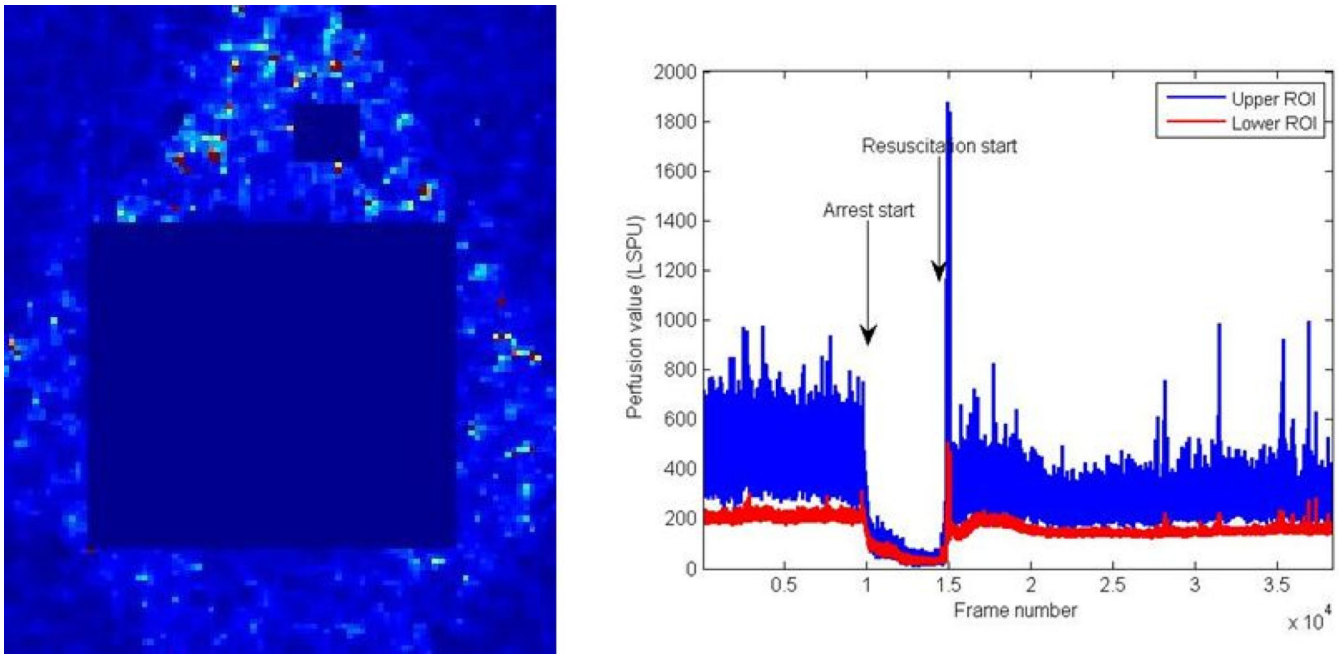

Fig. 8.

Left panel: LSCI perfusion map representing a large area of the cortex for a 17 day old rat. The two blue squares represent two ROIs. Right panel: time evolution of the perfusion in the two ROIs shown in the left panel. Asphyxial cardiac arrest starts around frame 9300; the resuscitation starts around frame 14700; return of spontaneous circulation is seen in frame 14879.

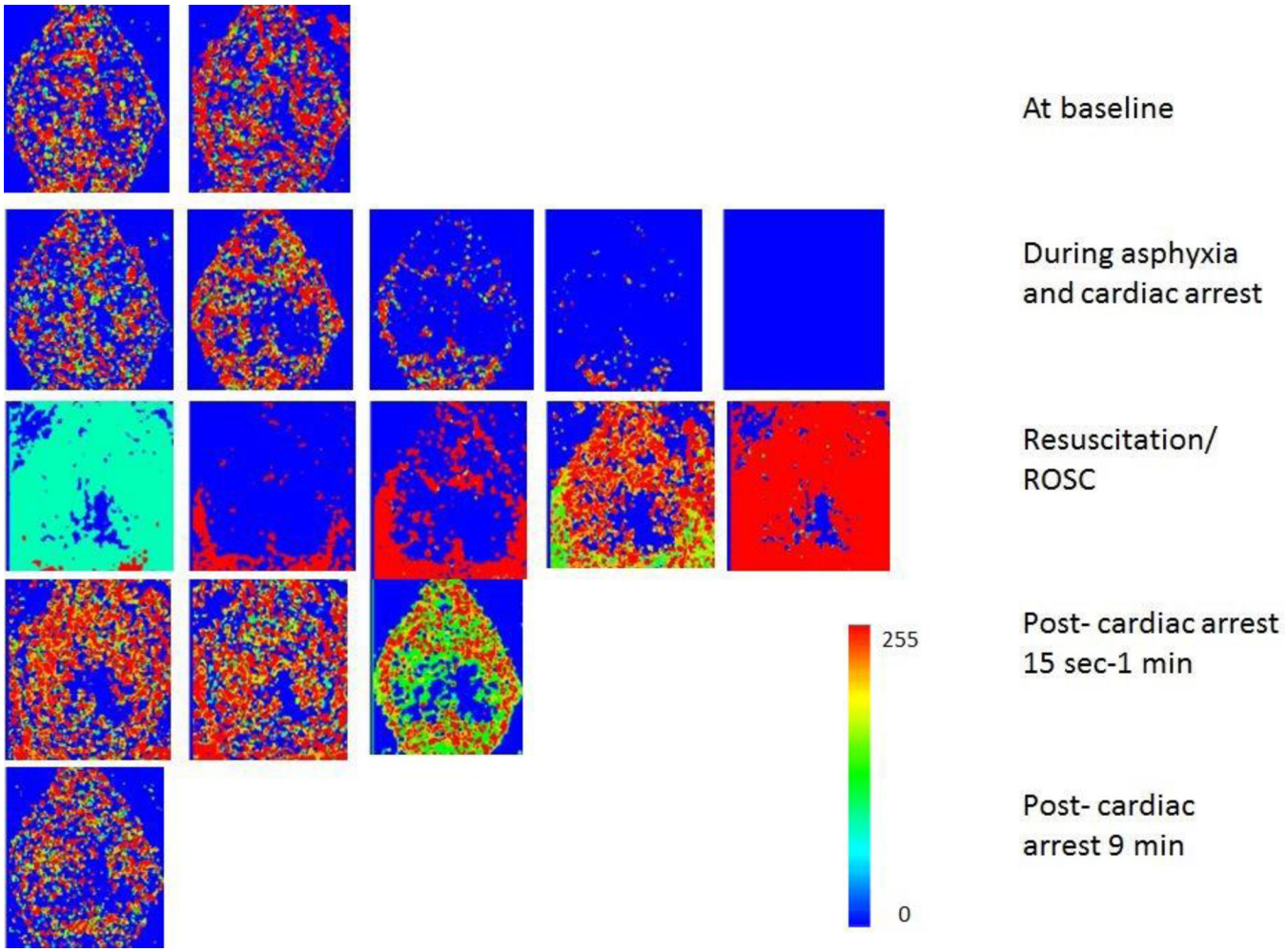

Fig. 9.

MHIs showing the fluctuations in regional cerebral blood flow of a rat. The perfusion variations are induced by asphyxia followed by cardiac arrest and resuscitation. Each MHI has been computed from a stack of LSCI perfusion images around a particular time point shown in Fig. 7. For the computation of each MHI, the buffer size was 6, and the threshold value was 20.

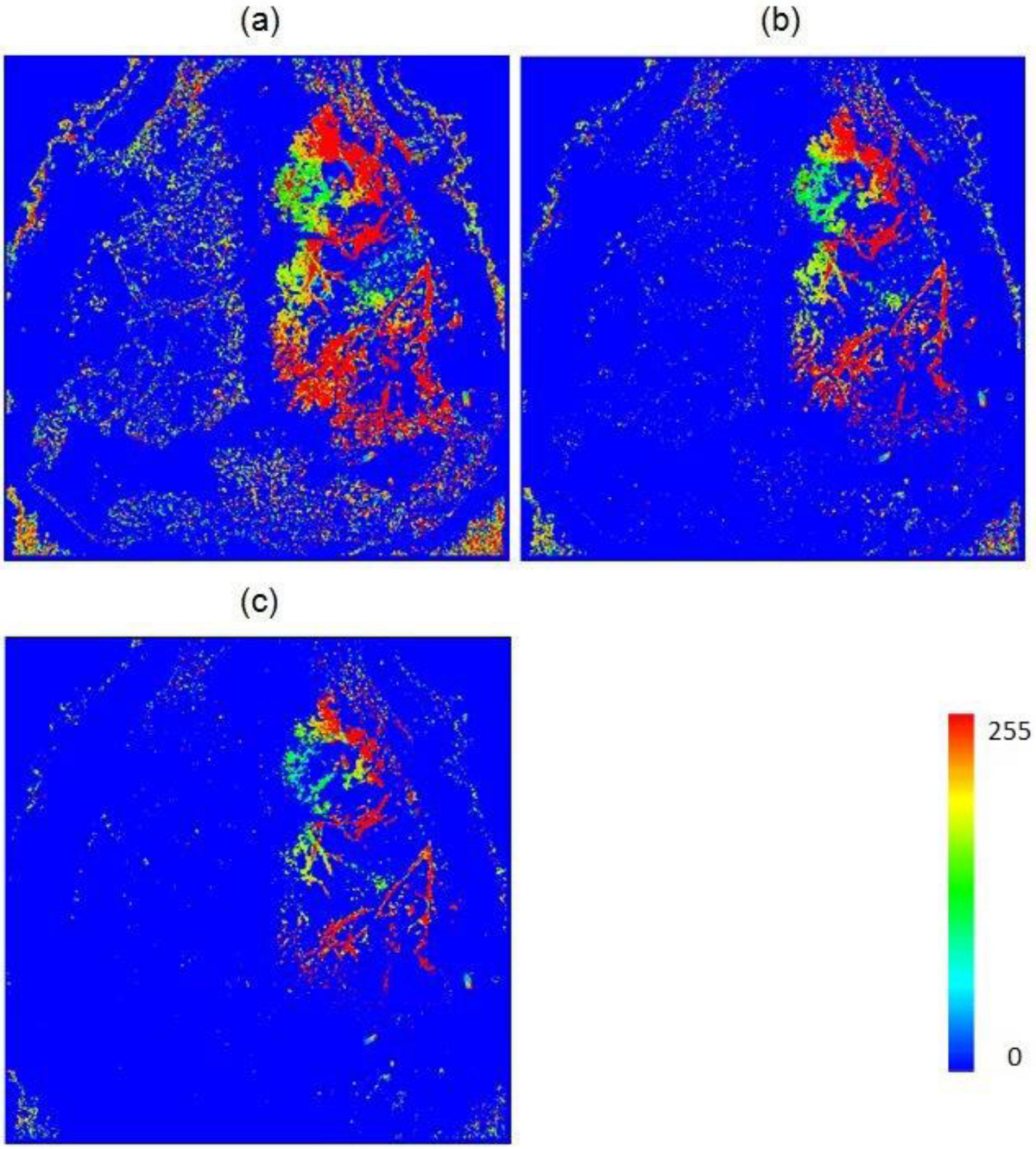

Fig. 10.
MHIs generated with different threshold values and with a buffer size of 6. The threshold value is equal to (a) 40; (b) 60; (c) 80.

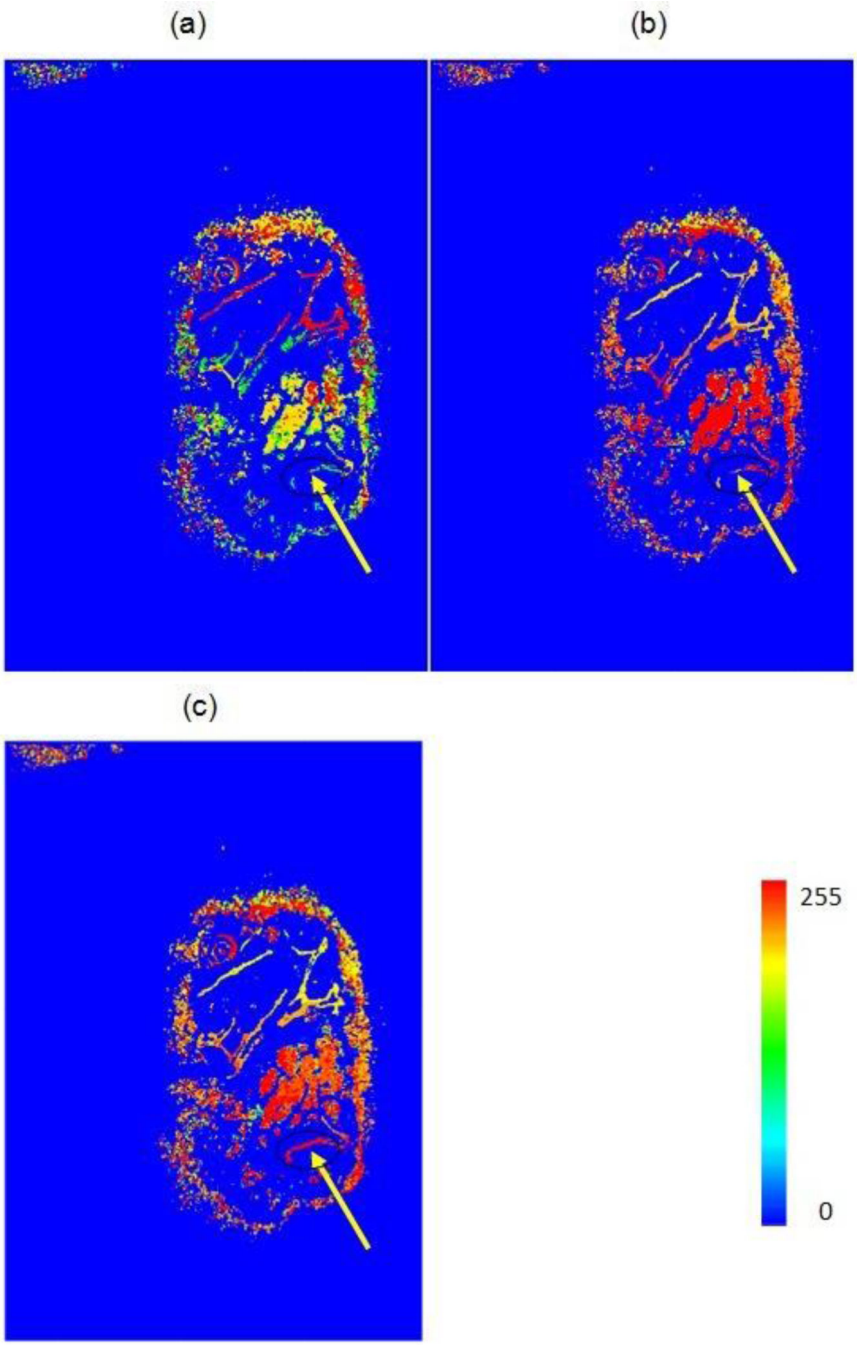

Fig. 11.

MHIs generated with different buffer sizes with a threshold of 60. The buffer size is equal to (a) 4; (b) 10; (c) 12. The arrow shows a region with low activities.